ACTA ACUSTICA UNITED WITH ACUSTICA
Vol. 90 (2004) 335 – 348

Acoustical Parameters for the Characterisation of the Classical Guitar

T. J. W. Hill*, B. E. Richardson†, S. J. Richardson
Department of Physics and Astronomy, Cardiff University, P.O. Box 913, Cardiff, CF24 3YB, Wales, UK

Summary
This paper shows how the input admittance of a guitar and its sound-pressure response at an arbitrary point in its radiation field can be characterised and reconstructed using a small set of acoustical parameters. These parameters comprise the resonance frequencies, Q-values, effective masses and orthogonal radiation components of a small number of low-order body modes. Details are given of the experimental procedures for extracting the acoustical parameters, including the measurement and spherical-harmonic decomposition of sound fields. Data are presented for one classical guitar, which illustrate typical values of the parameters. The work highlights the importance of dipole radiation and demonstrates how certain low-order modes contribute to the average response of the instrument well above their resonance frequencies.

PACS no. 43.75.Gh

1. Introduction

The basic mechanical and acoustical functions of the guitar are now well understood, but there is still considerable interest in trying to determine which of its many measurable dynamical and acoustical features are indicative of its tone or playing qualities. An obvious starting point is to attempt to correlate the various prominent and recurring features observed in frequency response functions, such as input admittance or sound-pressure response, with subjective psychoacoustical assessment of the "sound quality" (e.g. see Meyer [1]). This sort of mapping is fraught with difficulties, however. Frequency response functions themselves are complicated and a casual examination does not make it clear whether a tall peak is due to the presence of an easily excited mode, a mode with a high Q-value, or contributions from neighbouring modes. Furthermore, a strong peak in the input admittance does not necessarily yield a strong peak in the sound-pressure response. Consequently, it is not a trivial matter to investigate the multidimensional perceptual space arising from a complex dynamical and acoustical system such as a guitar. Nor is it easy to relate features in these response curves to the practical aspects of the construction of an instrument.

In the development of any model of guitar function, it is necessary to identify, and preferably keep to a minimum, the parameters required to describe the key physical and perceptual features of the instrument and its sound. An important step was taken by Christensen [2], who presents a very strong case for the economy and usefulness of parametrising sound-pressure response functions into a simple data set comprising resonance frequencies, Q-values, effective masses and monopole source strengths for a number of low-order modes of the guitar. The primary advantage of Christensen's model is that the output characteristics of the guitar are described by a straightforward linear sum of damped, simple-harmonic oscillators. This model was extended by Brooke [3] and Wright [4] and used for generating guitar tones which formed the basis of a set of psychoacoustical experiments investigating the relative importance of these various "acoustical parameters". This work showed that variations in the effective masses of certain principal modes had a significant effect on the "global" acoustical properties of instruments, whereas variations in mode frequencies were found, contrary to popular belief, to be of less importance, producing only "local" changes [4, 5]. In the light of these experiments, the principal motivation for undertaking the work presented here was to expand current understanding of the complex radiativities of guitars and to measure sets of acoustical parameters for a range of high-quality instruments (e.g. those made by renowned makers or chosen by performers). This paper concentrates primarily on presenting the methods with examples of measurements from one guitar; data from the other instruments investigated will be published at a later stage (preliminary reports are given in [6, 7, 8, 9]).

Few studies have been undertaken to quantify the radiation characteristics of stringed musical instruments. This is particularly true of the guitar, where radiation fields are generally inferred from studies of mode shapes rather

Received 17 September 2002,
accepted 15 October 2003.

* Current address: Acoustics Research Group, DEME, Open University, Walton Hall, Milton Keynes, MK7 6AA, UK

† Email: RichardsonBE@cardiff.ac.uk

than actually measured (e.g. see Caldersmith [10, 11] or Richardson [12]). Berge *et al*. [13] have undertaken a small number of measurements of sound fields from guitars and shown how computationally efficient techniques can be used for modelling radiation fields. Similarly, Brooke [3, 14] used boundary-element techniques to model sound fields, which demonstrated the directional nature of the radiation patterns associated with most modes. Near-field acoustical holography has also been used successfully for measuring sound fields of guitars [15] and violins [16], but this technique is usually confined to locating acoustical sources and sinks on the radiating structure.

Weinreich and co-workers have investigated various techniques for measuring sound radiation from violins. They used either direct or reciprocal methods. In direct experiments, the sound fields are measured in response to steady-state or impulsive excitation applied to the instrument. The measured fields can then be broken down into either a multipole or a spherical-harmonic expansion [17, 18]. Reciprocal methods insonify the structure with a specific sound field (usually restricted to monopole or dipole). The various responses at the bridge are then measured as a function of frequency [19, 20]. This method detects the aggregate response of all modes excited. Weinreich stresses the importance of the directivity of radiation in the development of violin tone colour [21].

The approach taken in this paper is to measure the key dynamical and acoustical parameters for each mode. The guitar is treated as a linear input-output system using an extended version of Christensen's model, incorporating damped, simple-harmonic oscillators driving monopole and dipole radiators. It is shown that this leads to a significant improvement in the reconstruction of sound-pressure response functions and also provides information on the input admittance seen by the string. This is indicative of an improvement in the characterisation of the instrument. Furthermore, it shows that the particular choice of dynamical and acoustical parameters are those which describe the key features in the acoustical performance of the instrument.

2. Theory

In Christensen's model [2], each mode of the guitar which has a significant response when driven at the bridge is represented by a mass-spring-damper system connected to a piston. The system is confined to a single degree of freedom and represents the response of the guitar driven by a vertically polarised, transverse vibration of the string. The attached piston is assumed small enough that it acts as a simple source of sound of source strength S_ω. The resulting pressure radiated by an individual mode to a position r in space when driven by a harmonic force $F\mathrm{e}^{-\mathrm{i}\omega t}$ is thus given by

$$p(r,\omega,t) = \frac{-\mathrm{i}\rho_0 ck}{4\pi r} S_\omega \mathrm{e}^{\mathrm{i}(kr-\omega t)}, \tag{1}$$

where ρ_0 is the density of the air, c is the speed of sound in air and $k = \omega/c$ is the wavenumber [22]. In this case, $S_\omega = U_0 A$, where U_0 is the velocity amplitude and A the effective area of the piston. In practice, S_ω can be obtained by integrating the velocity distribution of the mode over the vibrating surfaces of the instrument (including the "plug of air" in the soundhole).

The radiated sound pressure shows prominent peaks at mechanical resonances of the instrument where the admittance, or mobility, is a maximum. The admittance, $\mathcal{Y}(\omega)$, of an individual mode is given by

$$\mathcal{Y}(\omega) = \frac{U_0}{F} = \frac{\mathrm{i}\omega}{M(\omega^2 - \omega_0^2 + \mathrm{i}\omega_0\omega/Q)}, \tag{2}$$

where M is the effective (or equivalent) mass at the excitation point, Q is the Q-value of the resonance and ω_0 $(= 2\pi f_0)$ is the resonance frequency. This can be combined with equation (1) to give an expression for the sound pressure per unit force radiated by an individual mode:

$$\frac{p(r,\omega)}{F} = \frac{\rho_0}{4\pi r}\frac{A}{M}\frac{\omega^2}{(\omega^2 - \omega_0^2 + \mathrm{i}\omega_0\omega/Q)}\mathrm{e}^{\mathrm{i}kr}. \tag{3}$$

Christensen showed how the sound-pressure responses of guitars could be modelled in the low-frequency range (up to about 600 Hz) by summing equation (3) over several low-order modes. Using a process of trial and error (and fitting by eye), Christensen extracted approximate values for f_0, Q and the ratios A/M from sound-pressure response curves measured on five guitars. Note that to obtain separate values for A and M would have required measurements of both sound-pressure response and input admittance.

To extend Christensen's model to include dipoles and fields of higher order it is necessary to incorporate angular solutions in the radiated sound pressure. Acoustic waves radiating from a vibrating body in free space satisfy the Helmholtz wave equation

$$\nabla^2 p = \frac{1}{c^2}\frac{\partial^2 p}{\partial t^2}. \tag{4}$$

Solutions of this equation in spherical coordinates are well known. Equation (5) below shows that a complex pressure field $p(r,\theta,\phi)$ from an arbitrary out-going wave can be expressed as a sum of spherical harmonics, $Y_{lm}(\theta,\phi)$, spherical Hankel functions, $h_l(kr)$, and complex coefficients, a_{lm} [17, 22]. In this equation l is the order and m is the degree of the spherical harmonic.

$$p(r,\theta,\phi) = \sum_{l=0}^{\infty}\sum_{m=-l}^{l} a_{lm} Y_{lm}(\theta,\phi) h_l(kr). \tag{5}$$

There is some variability in the definition of $Y_{lm}(\theta,\phi)$ in the literature, so it is appropriate to state it explicitly. For $m \geq 0$,

$$Y_{lm}(\theta,\phi) = \left[\frac{2l+1}{4\pi}\frac{(l-m)!}{(l+m)!}\right]^{\frac{1}{2}} (-1)^m \cdot P_l^m(\cos\theta)\,\mathrm{e}^{\mathrm{i}m\phi}, \tag{6}$$

where the $P_l^m(\cos\theta)$ are associated Legendre functions. The numerical values defined by the first term represent the normalising coefficients, N_{lm}, and the second term is a "phase factor". For negative values of m, $Y_{l-m} = (-1)^m Y_{lm}^*$.

To appreciate how fields of higher order are incorporated into the model, it is instructive to take two special cases. The monopole field radiated by Christensen's model is described by equation (5) with $l = m = 0$. Comparison with equation (3) shows that the monopole coefficient, a_{00}, is given by

$$a_{00} = \frac{1}{N_{00}} \frac{\rho_0 c k^2}{4\pi} AF\mathcal{Y}(\omega), \tag{7}$$

where $AF\mathcal{Y}(\omega) \equiv S_\omega$, the monopole source strength. Next consider a mode of the guitar which radiates a pure dipole field. Since the dipole can have an arbitrary orientation in space, assume that this particular field is aligned along the z-axis; this is a convenient choice since it then has a direct counterpart described by equation (5) with $l = 1$ and $m = 0$. A similar comparison gives

$$a_{10} = \frac{1}{N_{10}} \frac{\rho_0 c k^3}{4\pi} G_{10} F\mathcal{Y}(\omega), \tag{8}$$

where $G_{10}F\mathcal{Y}(\omega)$ is equivalent to the dipole source strength. The coefficients a_{lm} thus incorporate details of the mechanical response of the instrument as well as the source strengths of the different field components. A general expression for the resultant pressure amplitude per unit applied force radiated by an individual mode, which incorporates radiation components of higher order, can be written as

$$\frac{p(r,\theta,\phi,\omega)}{F} = \sum_{l=0}^{\infty} \sum_{m=-l}^{l} \frac{\rho_0 c}{4\pi} k^{(l+2)} G_{lm}\, \mathcal{Y}(\omega) \cdot P_l^m(\cos\theta)\, \mathrm{e}^{\mathrm{i}m\phi}\, h_l(kr). \tag{9}$$

In the above equation, the G_{lm} are the weights of the orthogonal radiation components for an individual mode. (The product $G_{lm}\mathcal{Y}(\omega)$ is basically the same as the radiativity function $\Gamma_{lm}(\omega)$ introduced by Weinreich [19].) From equation (7) it is clear that G_{00} is equivalent to A. Similarly, the G_{1m} can be shown to be equivalent to the effective area of the dipole's component simple sources multiplied by the distance between them. Removing the normalisation coefficient and phase factor from the spherical harmonics in equation (9) has the advantage of scaling the fields such that dipoles of equal source strengths aligned along the x-, y- and z-axes generate Gs of equal magnitude. Although there is a one-to-one correspondence between the spherical-harmonic description and some of the higher order multipoles (e.g. the tesseral quadrupoles), these fields require additional scaling if the same comparisons are to be made [22]. However, multipoles are not an orthogonal set and most higher order multipoles require a combination of spherical harmonics for their description. As the geometrical complexity of the radiating body and the frequency at which it is driven increase, radiation components of higher orders and degrees become more significant. In these circumstances, the use of orthogonal radiation components is preferred, and the particular scaling is then immaterial.

The weights G_{lm} for *individual* modes are extracted by spherical-harmonic decomposition of measured sound fields. This procedure requires careful choice of driving positions such that the instrument, when driven at resonance, is vibrating predominantly in a single mode (see Section 3.2). In addition, curve-fitting techniques are used to extract values of f_0, Q and M for each mode from measurements of input admittance at the bridge (see Section 4.2). This set of "acoustical parameters" can then be used to reconstruct the input admittance seen by the strings using equation (2) or, on the assumption that the G_{lm} are constant across a fairly broad frequency range, to reconstruct the radiated sound field using equation (9). In each case, the equations are summed over the range of modes of interest.

3. Sound-field measurements and decomposition

3.1. Spherical-harmonic decomposition

The procedure for determining the G_{lm} is based on a method described by Weinreich and Arnold [17], which requires measurements of sound fields to be made over the surfaces of two spheres surrounding the source (Figure 1) so that both out-going and in-coming waves can be separated. Equation (5) showed that in the case of a simple outgoing wave the radiated complex pressure measured on the surface of a sphere can be expressed as a weighted sum of the product of spherical harmonics and spherical Hankel functions. Real measurements, however, are always contaminated by reflected and scattered waves, the latter being particularly troublesome in the near field. The fields on the measurement spheres then comprise both out-going and in-coming wave components, as described by the following equation, in which b_{lm} would be zero only in "ideal" conditions:

$$\frac{p(r,\theta,\phi)}{F} = \sum_{l=0}^{\infty} \sum_{m=-l}^{l} C_{lm}(r)\, Y_{lm}(\theta,\phi) = \sum_{l=0}^{\infty} \sum_{m=-l}^{l} \left[a_{lm} h_l(kr) + b_{lm} h_l^*(kr)\right] Y_{lm}(\theta,\phi). \tag{10}$$

Spherical-harmonic decomposition is the process of determining the complex coefficients $C_{lm}(r)$ from a measured sound field $p(r,\theta,\phi)/F$. For a field measured at radius r, the coefficients are given by the following double integral:

$$C_{lm}(r) = \int_{\theta=0}^{\pi} \int_{\phi=0}^{2\pi} \frac{p(r,\theta,\phi)}{F} Y_{lm}^*(\theta,\phi) \sin\theta \,\mathrm{d}\phi \,\mathrm{d}\theta. \tag{11}$$

For the purposes of numerical evaluation this equation can be re-expressed as a Fourier transform in ϕ and an integration in θ, which can be evaluated using Gaussian quadrature [23]. For a predetermined number of θ-steps, Gaussian quadrature dictates the values of θ at which measurements must be taken and provides weights such that the integral is evaluated exactly by a discrete sum of weighted terms.

If measurements of the complex pressure are taken on two concentric spheres encompassing the source, such that (ideally) there are no sources or scatterers between the two spheres, then the complex coefficients a_{lm} and b_{lm} of the out-going and in-coming wave components are given by solutions of the following matrix equation (see [17, 24]):

$$\begin{bmatrix} a_{lm} \\ b_{lm} \end{bmatrix} = \begin{bmatrix} h_l(kr_1) & h_l^*(kr_1) \\ h_l(kr_2) & h_l^*(kr_2) \end{bmatrix}^{-1} \begin{bmatrix} C_{lm}(r_1) \\ C_{lm}(r_2) \end{bmatrix}. \qquad (12)$$

In anechoic conditions, or assuming negligible in-coming wave components, the weights of the orthogonal spherical radiation components for an individual mode at resonance are then given by

$$G_{lm} = N_{lm} \frac{4\pi}{\rho_0 c} k^{-(l+2)} \frac{M\omega_0}{Q} a_{lm}. \qquad (13)$$

3.2. Experimental procedure

The guitar was located in the middle of a semi-anechoic chamber, of working dimensions $2.2 \times 2.2 \times 1.5\,\mathrm{m}^3$ (wedge size 0.55 m), and positioned such that the origin of the measurement system lay near the centre of the body (approximately midway between the bridge and the soundhole, as shown in Figure 1). The instrument was "freely" suspended on a rotating column by cotton tape and elastic bands at the headstock with gentle restraint in the lower bout and with the strings damped. The instrument was driven at resonance using a small magnet-coil driving system (with the magnet attached to the guitar). The sound fields were measured with a pair of B&K $1/2$-inch condenser microphones located on a rotating boom. The combined movements of the support column and boom effectively allowed pressure measurements to be made on the surfaces of two concentric spheres.

Figure 2 shows a schematic diagram of the measurement instrumentation. The guitar was rotated about the vertical axis in $36 \times 10^\circ$ steps and the boom positioned the microphones at nine angles prescribed by the Gaussian quadrature at constant radii of 0.45 m and 0.71 m. The motion of the stages was computer controlled with measurement positions located positively using slotted IR detectors sensing holes in a pair of discs.

The instrument was excited at each of the resonance frequencies of interest. An important aspect of this work is that we have endeavoured to determine the sound fields associated with individual modes. In practice, it is not usually possible to isolate and excite individual modes of a complex system, but holographic and speckle interferometric studies of each instrument allowed single or multiple driving positions to be chosen which strongly excited one mode with minimal perturbation from other modes. The basic criterion for separation is that the observed mode shape should not change its character when sweeping through the resonance frequency [25].

The 9×36 measurement mesh was a compromise which allowed good graphical resolution of the sound fields whilst avoiding restrictions imposed by the physical set-up and size of chamber. The mesh also produced convenient measurement positions on both the x- and y-axes and gave

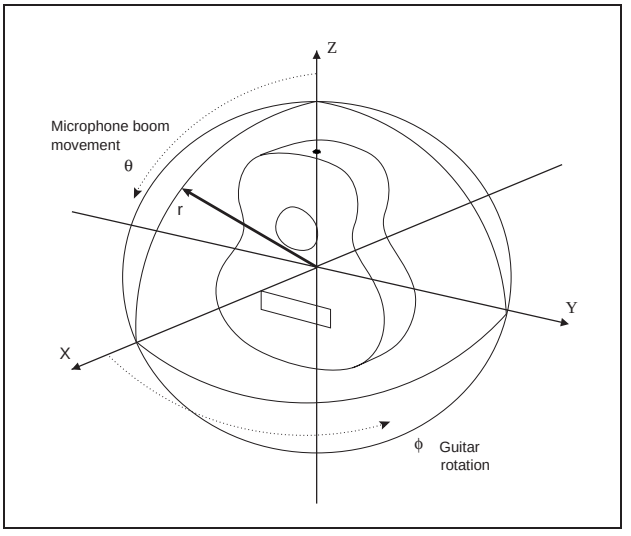

Figure 1. Sound-field measurement coordinate system. The figure shows only one of the "measurement spheres". The pair of microphones sample the sound field at various coordinates θ and ϕ at two fixed radii.

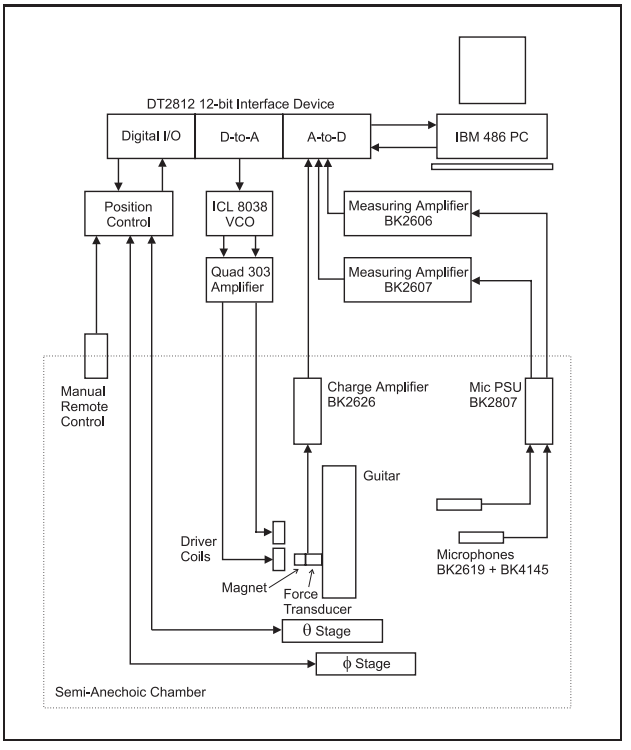

Figure 2. Apparatus used for sound-field measurements with manufacturers' component numbers.

good decomposition accuracy. The spherical-harmonic decomposition and extraction of the C_{lm} was performed using a vector-matrix algorithm written in MatLab [26]. The nature of the algorithm is such that it is possible to extract only 49 sequential values of C_{lm} (up to $l = 6$). Since terms of higher order are susceptible to measurement noise, the system was deliberately over-determined [27]. For sound fields presented in this paper, spherical-harmonic coefficients were restricted to a maximum of third order (equivalent to octupoles) since higher orders were deemed insignificant.

The decomposition is unable to extract reliably the phases of the orthogonal radiation components. This is because the algorithm uses a spherical-wave decomposition which treats the guitar as an ensemble of point sources rather than as a radiator of finite extent. One of the benefits of such an approach is that the sources must be either in or out of phase, whereas in the case of a radiator of finite extent the phase would be a continuous variable. Procedurally, this meant that equation (13) was used to calculate only the magnitude of the G_{lm}. The polarities were subsequently determined by trial-and-error fitting to measured sound-pressure response curves (amplitude and phase). The latter were measured on both radii in three directions using a combination of the sound-field and admittance apparatus.

4. Admittance measurements

4.1. Input admittance

Several methods have been used for measuring the admittance of stringed musical instruments, such as steady-state sinusoidal excitation [28], impulse-hammer excitation [29, 30] and reciprocal excitation [31]. The former method was used here because it was compatible with our procedures for measuring sound fields and with the holographic techniques used for visualising mode shapes. The method produces quasi-continuous, calibrated frequency response curves, from which modal parameters can be extracted.

The instrument was excited using a magnet-coil assembly. The excitation force and velocity response at the bridge were measured using an "impedance head", comprising a custom-built piezoelectric force transducer and a miniature accelerometer, as shown in Figure 3(b). The mass of the impedance head, including the magnet, was approximately 3.5 g. Although configuration (a) is preferred [32], because the accelerometer is mounted directly on the structure, configuration (b) is far more convenient because of restricted access to the inside of instruments; the two methods gave identical results when the increased seismic mass of the force transducer was taken into account. The force transducer was calibrated by attaching it and a calibrated accelerometer to opposite ends of a freely suspended test mass and measuring their response to sinusoidal excitation [32]. The advantage of this method is that it calibrates the entire system. Subsequently, it is necessary only to replace the calibration block with the structure under investigation.

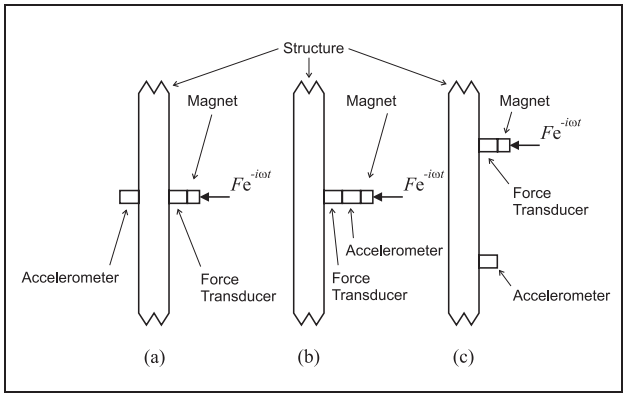

Figure 3. Alternative configurations for mounting the force transducer and accelerometer (a) on either side of the structure, (b) back-to-back (an "impedance head"), and (c) transfer admittance.

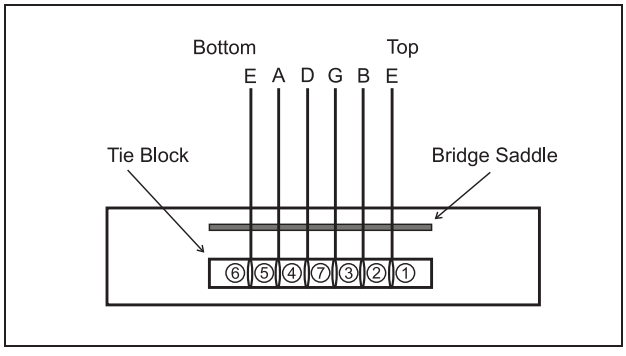

Figure 4. Measurement Positions 1 to 7 on the guitar bridge.

Rather than devise special mounts to fit over the bridge saddle, admittance measurements were made by attaching transducers to the tie block (Figure 4). Admittance data were collected at each of the numbered positions, but data are presented for Position 1 only. Transducers were attached to the structure with double-sided tape. Experiments showed that in the frequency range of interest, this was just as effective as gluing them. All admittance experiments were carried out in the semi-anechoic chamber using supports and constraints similar to those described in Section 3.2.

4.2. Parameter extraction

Figure 5 shows the instrumentation used for the admittance measurements. The digital-to-analogue output of a PC interface card (Data Translation DT2801A) was used to sweep an ac signal from a voltage-controlled oscillator in logarithmic frequency steps. The force and acceleration signals were then sampled and an FFT used to determine the frequency, amplitude and relative phase of the force and acceleration signals, from which the admittance was calculated.

Various schemes for extracting modal parameters were assessed, including circle fitting and a method advocated

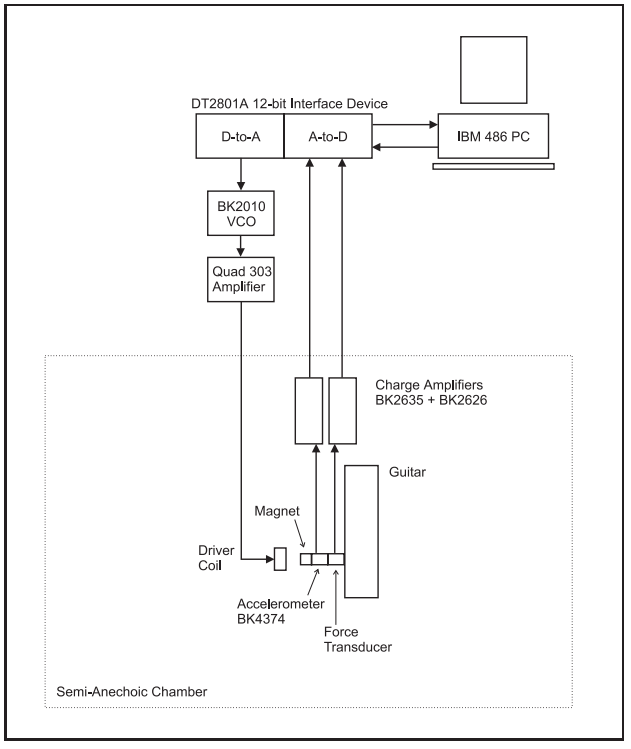

Figure 5. Apparatus used for input-admittance measurements.

by Arnold and Weinreich [18]. However, since the peaks were usually well separated, a variation of the simple peak-picking (or peak-amplitude) method [32] was found to be perfectly adequate and used to extract values of f_0, Q and M for each mode. This involved selecting individual peaks in the admittance amplitude data and curve-fitting to equation 2 using a least-squares minimisation. Working from low to high frequencies, each resonance was fitted in turn using points around each peak and data from previous resonances.

4.3. Transfer admittance

The data for acoustical parameters shown in this paper are those measured at excitation Position 1 at the bridge. However, the effective mass of a mode varies from point to point over the structure. This has important consequences for the determination of the G_{lm} because procedurally it is sometimes necessary to excite the instrument at points away from the bridge. Under these circumstances, the extracted value of the G_{lm} must be scaled appropriately.

A transfer admittance relates the velocity at one point on the structure to the force applied at another. Let the displacement amplitudes at two points on the structure when vibrating in one of its modes be ψ_1 and ψ_2. Simple energy considerations show that the mass-like term extracted from a transfer admittance, M_T, is proportional to $1/\psi_1\psi_2$. The effective mass is obtained when the excitation and observation points coincide; clearly M is proportional to $1/\psi_1^2$. Thus the ratio of ψ_1/ψ_2 is given by M_T/M. Since a particular G_{lm} is proportional to the displacement amplitude at the point of excitation, this factor can be used to scale the values as if the mode had been driven at the bridge.

Measurements of transfer admittance for scaling the G_{lm} were made using the same procedures described above but with the accelerometer and force transducers separated (Figure 3c). Note that M_T can be positive or negative depending on the relative phase of the two points. In addition, transfer admittances were measured between the different driving positions at the bridge to give a more complete picture of the response of the instrument.

5. Results

In this section we present data from one classical guitar (BR2) and show how the extracted acoustical parameters can be used to reconstruct frequency response functions. The guitar is hand-crafted with a spruce soundboard built to a traditional design with Torres fan-strutting. The acoustical and modal characteristics of this instrument are well known and documented from previous investigations (e.g. see Richardson [25]). Measured data included input admittance at the bridge, sound-field polar plots and sound-pressure response curves. Modal and spherical-harmonic decomposition was used to extract acoustical parameters for seven, prominent, low-order modes. Reconstructions of sound fields and response functions demonstrate the effectiveness of the theory and experimental techniques and also confirm the appropriateness of the chosen parameters in characterising the acoustical signature of the instrument.

Figure 6 shows the measured and reconstructed input admittance at the top E-string termination at the bridge. Of all the string positions, this is arguably the most important since the top string is used largely for melody. In instruments with symmetrical fan-bracing, as in this case, the responses measured at Positions 1 and 6 are often very similar, though the intermediate positions can vary quite considerably. Table I lists the values of f_0, Q and M for the first-seven prominent peaks. Figure 7 shows an example of a transfer admittance. Reconstructions of both this and the input admittance (using about 20 modes) show that the routine used for modal extraction was generally reliable in the range up to 1 or 2 kHz. Good fits to the peaks are essential for accurate determination of the G_{lm}. In the frequency range above 1 kHz modal overlap increases and the method becomes less useful.

Measured sound fields are shown in Figure 8. Each panel shows a holographic interferogram of a mode, its resonance frequency and the associated sound field. The interferograms basically show contour maps of the displacement amplitude of the structural vibrations, in which the brightest fringes are nodes. Different mass loading in the various experiments is responsible for the small discrepancy between the mode frequencies quoted here and in Table I. Modes of the body are complex, usually involving corporate motion of the soundboard, back plate, ribs and the air inside the cavity (e.g. see [12, 33]). However, purely as an aid to identification, it is convenient to name modes as (n_y, n_z) by counting "half-waves" across and along the active regions of the plates. The prefix *T* or

Table I. Resonance frequencies, Q-values, effective masses and the first four weights of the orthogonal radiation components for the principal low-order modes of Guitar BR2. Data for Position 1 at the bridge.

Mode	f_0 (Hz)	Q	M (kg)	G_{00} (m^2)	G_{1x} (m^3)	G_{1y} (m^3)	G_{1z} (m^3)
$T(1,1)_1$	94.3	58	0.378	−0.0220	−0.0093	−0.0014	−0.0124
$T(1,1)_2$	183.1	52	0.088	0.0155	0.0036	−0.0001	0.0003
$T(2,1)$	219.0	79	0.136	0.0005	0.0003	0.0036	0.0001
$B(1,2)$	227.0	30	0.450	0.0448	0.0045	−0.0007	0.0002
$T(1,2)_1$	363.1	82	1.287	0.0202	0.0014	−0.0003	0.0001
$T(1,2)_2$	418.1	32	0.299	−0.0262	−0.0043	−0.0001	−0.0010
$T(3,1)$	453.7	63	0.951	0.0089	−0.0013	0.0001	0.0032

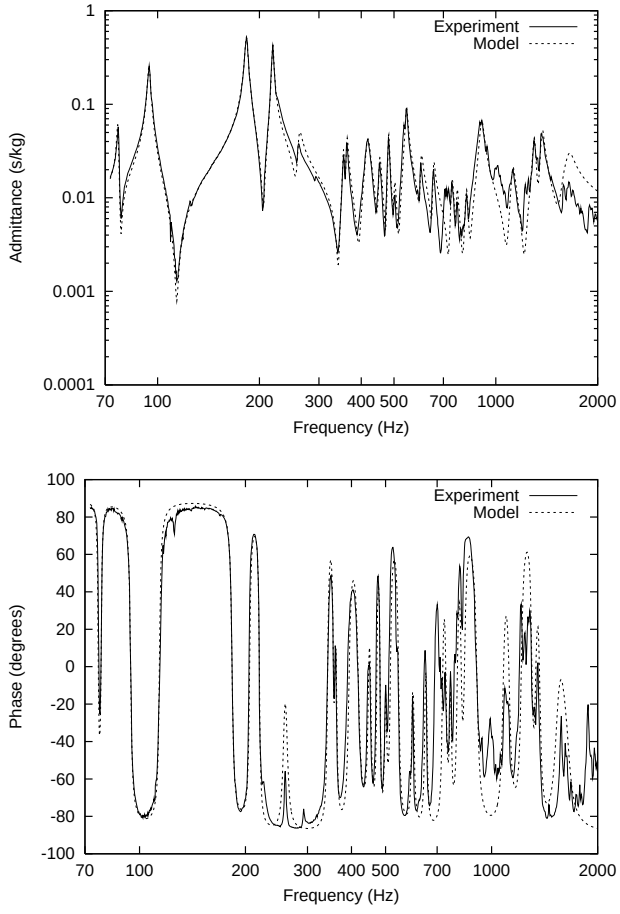

Figure 6. Input admittance at bridge Position 1. The solid line shows the measured data and the dotted line shows the reconstructed response.

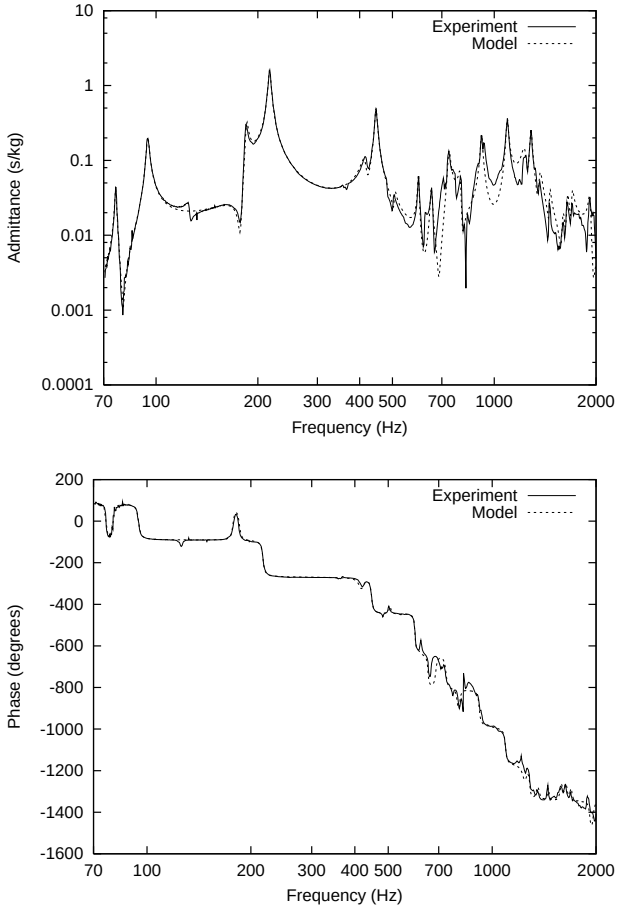

Figure 7. Transfer admittance between opposite ends of the bridge.

B is then used to identify the primary location of the motion depending on whether this lies in the soundboard (top plate) or back plate. Where more than one mode has a similar spatial distribution (which often occurs when there is significant coupling between structural and air-cavity motion), a subscript is used to differentiate between them. For reference, a comprehensive set of guitar modes up to about 1 kHz is shown and described by Richardson [12].

In Figure 8, the sound fields are plotted as conventional 3-D polar plots, in which the length of the radius vector is proportional to the pressure magnitude at each measurement location; the grey-scales are also used to show the field variations. The accompanying interferograms show the driving positions used for each measurement, but the plots have been scaled to show the fields produced by driving at the bridge (see Section 4.3). Since each plot shows the radiated pressure per unit excitation force, the figures show the comparative radiativity of each mode. The field plots appear to show little noise contamination and exhibit forms which are suggested by the underlying mode shapes, e.g. the $T(2,1)$ mode produces strong dipole radiation along the y-axis as would be expected from the an-

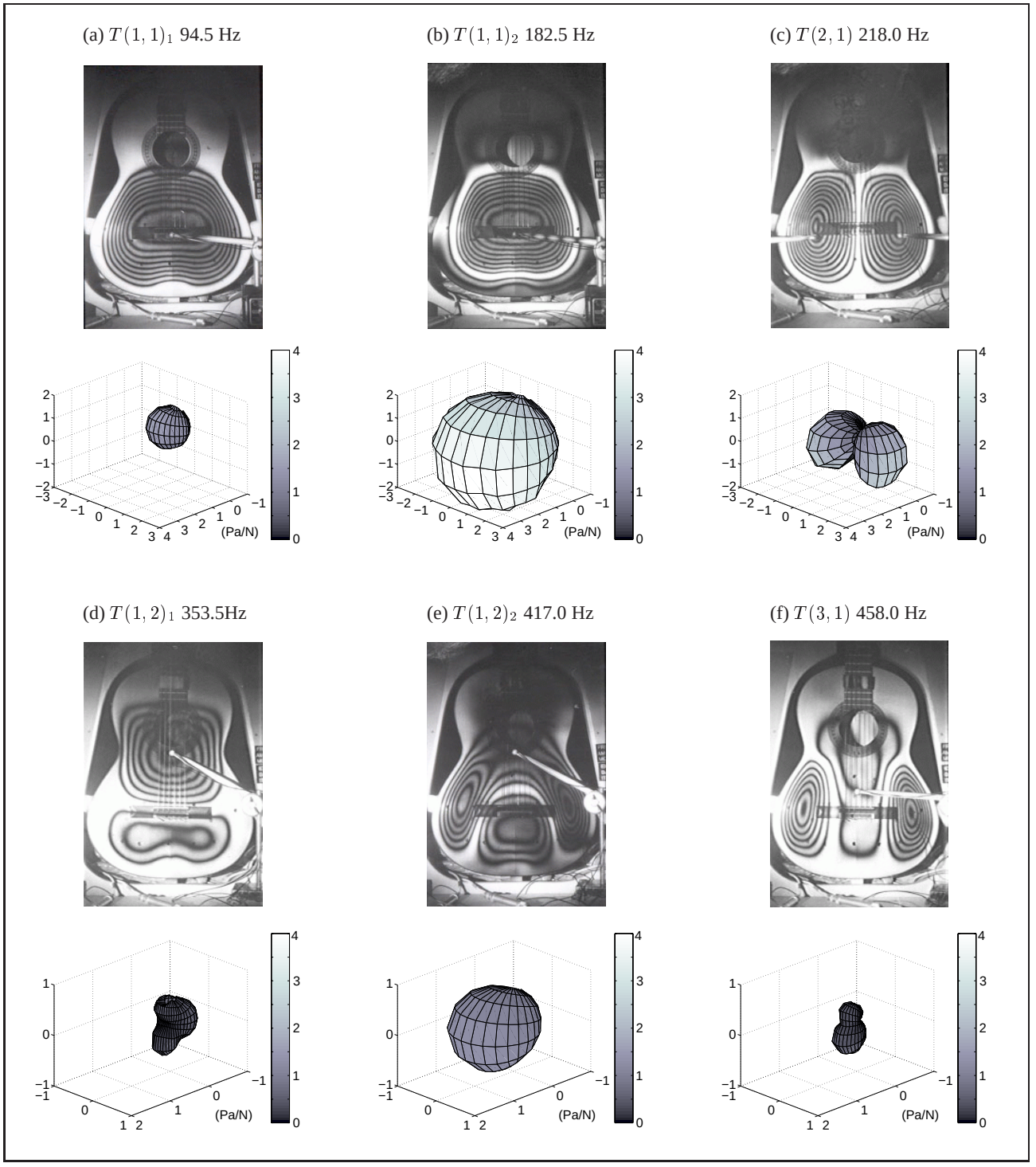

Figure 8. Holographic interferograms of six guitar modes and 3-D polar plots of their associated sound fields (Pa/N). Sound fields are shown for measurements on the inner sphere, of radius $r = 0.45$ m and scaled to show the radiativity when driven at the bridge. The fields are shown with the guitar orientated as in Figure 1. The amplitude of motion shown in the interferograms is arbitrarily chosen. Note the changes in scale between different plots.

tisymmetric motion of the soundboard. The complex pressure measurements of each field were decomposed into out-going spherical-harmonic wave components, which, when scaled by M_T/M, give the weights G_{lm} associated with driving at the bridge. Table I shows the magnitudes and polarities of the monopole component, G_{00}, and the three dipole components, G_{1x}, G_{1y} and G_{1z}; for convenience, the latter have been processed to resolve them along the x-, y- and z-axes. (Note that a dipole aligned along the z-axis has a field proportional to Y_{10}, and fields associated with dipoles aligned along the x- and y-axes are proportional to $\Re(Y_{11})$ and $\Im(Y_{11})$ respectively.) As mentioned in Section 3.2, the phases of the G_{lm} were not determined directly from the spherical-harmonic decom-

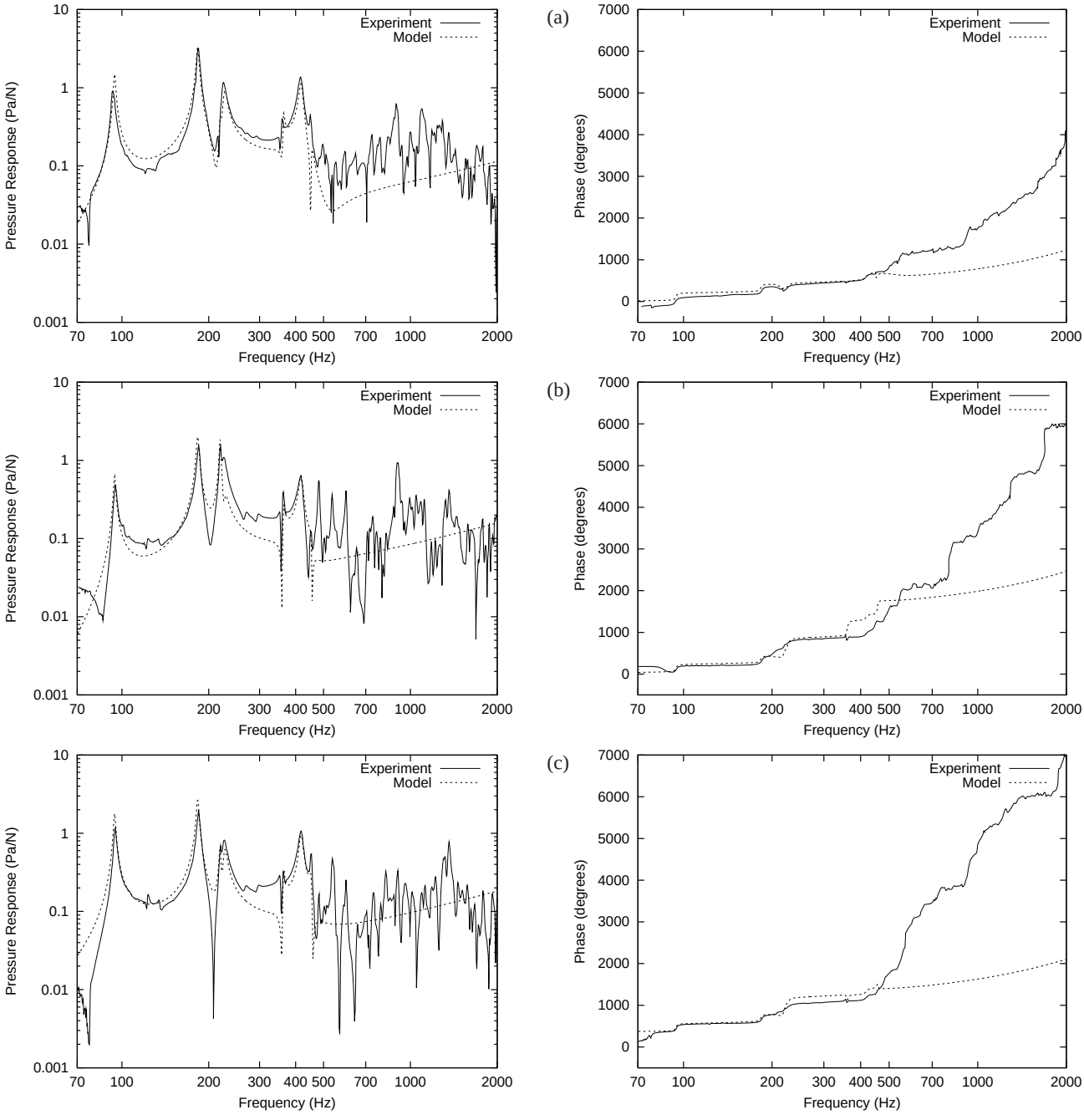

Figure 9. Measured and modelled sound-pressure response curves. Data are reconstructed using monopole and dipole components. (a) $r = 0.45$ m, $\theta = 90°$, $\phi = 0°$, (b) $r = 0.45$ m, $\theta = 90°$, $\phi = -90°$ and (c) $r = 0.45$ m, $\theta = 45°$, $\phi = -45°$.

position. Since the $T(1,1)_2$ usually radiates the strongest monopole component, the polarity of G_{00} for this mode was assumed positive (and there are other arguments to support this choice). Other polarities were then set to give the correct relative phases, as described previously.

Figure 9 shows the magnitude and phase of the sound-pressure response measured at three different positions to the front and side of the guitar. Because the radiation is directional, the heights of peaks vary at each location. For example, the antisymmetric $T(2,1)$ mode does not radiate significantly along the x-axis (Figure 9a) but it can be seen to contribute to one of a pair of peaks in the 220 Hz region in the other two figures. Response curves reconstructed from the parameters listed in Table I are shown as dashed lines. These clearly reproduce the main features in the frequency range 70–500 Hz, within which the principal modes lie. Discrepancies in the fits within this range are most likely caused by failure to include one or two weakly radiating modes. In the frequency range above 600 Hz the model appears to predict the baseline, or average pressure response. This will be discussed further in Sections 6 and 6.2. The mismatch in the modelled phase is thought to be the result of small but unavoidable scatter in the near field and also a consequence of using a model comprising point sources. Overall, however, it appears that the small data set is able to characterise the system quite effectively.

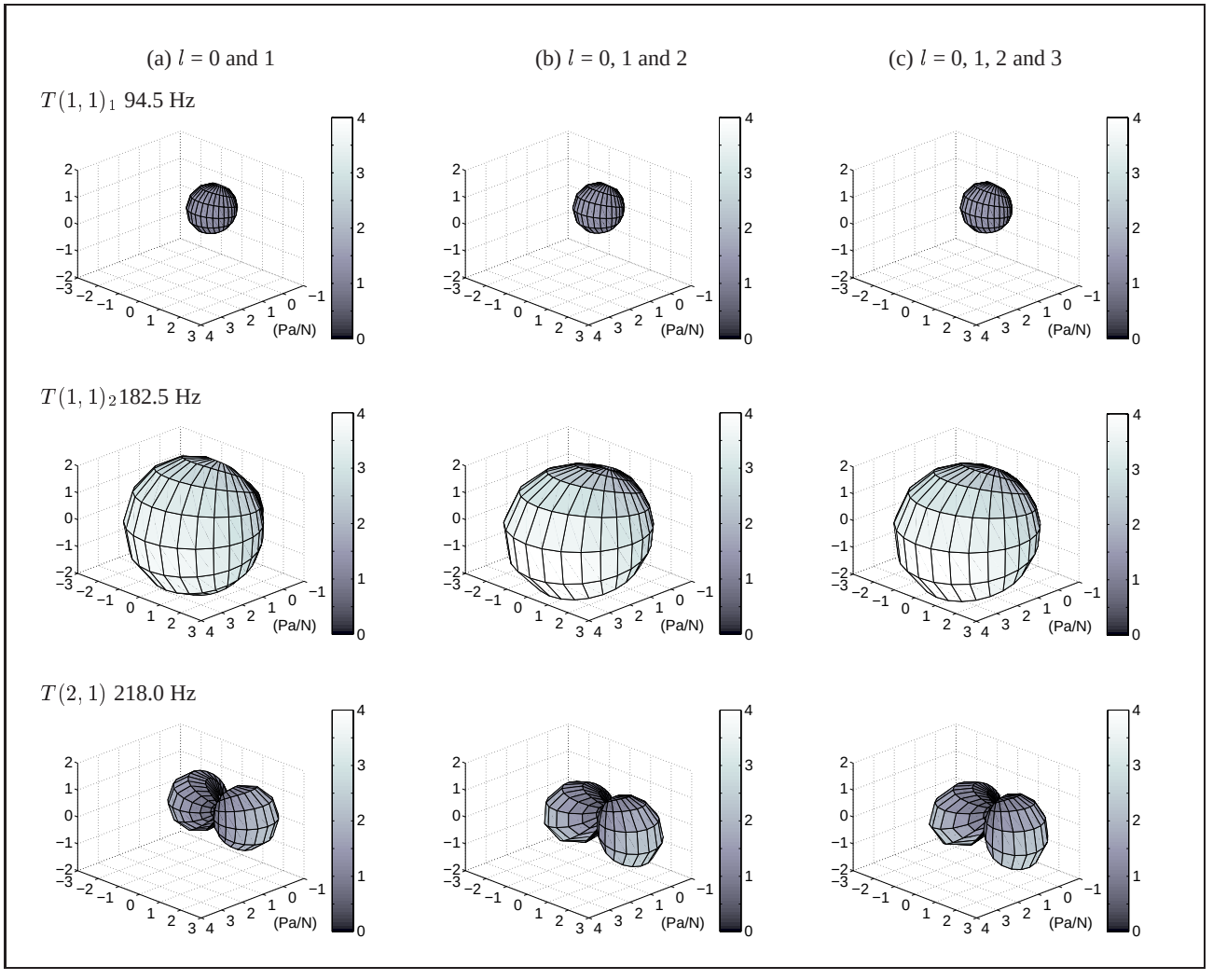

Figure 10. Reconstructions of the sound fields shown in Figure 8 using sequential addition of spherical harmonics and spherical Hankel functions of orders (a) $l = 0$ and 1, (b) $l = 0$, 1 and 2, and (c) $l = 0$, 1, 2 and 3. The fields are reconstructed from data specifying both out-going and in-coming waves.

6. Discussion

6.1. Monopole and dipole components

The acoustical parameters determined for Guitar BR2 are representative of those found in Torres-braced classical guitars (and the mode shapes and resonance frequencies are comparable with data published in the general literature). It is useful to compare these parameters with data collected by Christensen [2], since his values of A/M are equivalent to the ratios G_{00}/M. When reconstructing sound-pressure response curves, Christensen chose to ignore the "air resonance", the first strong peak which occurs around 100 Hz in all guitars. Although much of the radiation at this resonance is generated from movement of the "plug of air" in the soundhole [34], there is no reason to exclude modal data for this resonance from the set of acoustical parameters. Christensen was unable to identify positively which mode created each peak, but undoubtedly the first mode reported in each of his five data sets would be equivalent to the $T(1,1)_2$ mode of this study. Christensen's A/M values for this mode are consistently high compared with our measurements, which we attribute in part to his underestimate of Q-values (his quoted values are systematically low compared with most published data) and the absence of both dipole components of the radiation field and information on the lowest resonance. Our chosen set of instruments also shows a much wider range of mode frequencies [8] than those reported by Christensen.

Although the monopole components clearly dominate the radiation fields, the dipole components are certainly significant. Indeed, one of the surprises of this project as a whole has been the strengths of some of the dipole components associated with low-order modes such as the $T(1,1)_1$, $T(1,1)_2$ and $B(1,2)_1$ (e.g. see further data in [8]). These are often described as "air-pumping" modes, with the implication that they have omni-directional fields, but it is clear from Table I that all three have a relatively strong dipole component along the x-axis (front to back). In the low-frequency range of most guitars (including Guitar BR2), interaction between the structural mo-

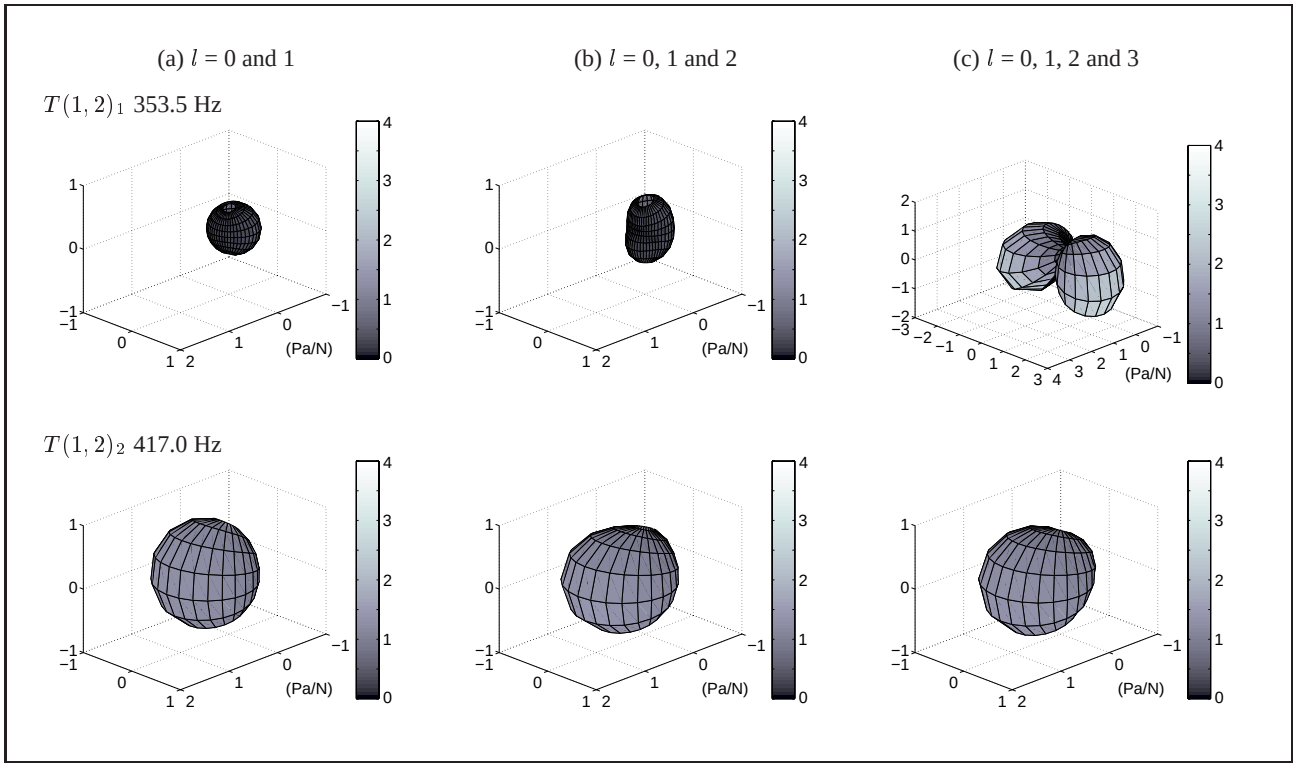

Figure 10. Continuation.

tion of the soundboard and back plate and the air in the ported cavity create a resonance triplet [12, 35], and it is the relative magnitude and phase of radiation from each of these "component parts" which dictates the strength of the monopole and dipole radiation. In addition, the $T(1,1)_1$ mode has a relatively strong dipole component along the line of the strings (z-axis), no doubt created by out-of-phase motion of the soundboard in the bridge area and of the air in the soundhole.

As expected from their increasing complexity, modes of higher order showed greater directionality. However, radiation components with orders greater than $l = 1$ were not particularly significant. Figure 10 shows reconstructions of sound fields using terms of successively higher order. Whilst it is clear that the higher order spherical harmonics are required for adequate reconstruction of the field associated with the $T(1,2)_1$ mode, for example, it turns out that this particular mode contributes little to the instrument's response because the string terminations lie very close to a nodal line (i.e. its effective mass at the bridge is large). We conclude, however, that monopole and dipole terms are a minimum requirement to characterise sound radiation from guitars.

Partly because of the difficulty of isolating and measuring radiation fields associated with higher modes, parameters were extracted for a small number of low-order body modes only. Although this limited set is incapable of reproducing detail above about 600 Hz, corporately it appears to set the baseline for the response in the mid-frequency range (600–2000 Hz), thus supporting the argument that a small number of low-order modes have an influence on the overall quality of the instrument (e.g. see [1, 4, 5, 36]). Combining equations (2) and (9) shows that when the excitation frequency exceeds the resonance frequencies of these modes, and this is true for the vast majority of the overtones of plucked guitar strings, the monopole radiation tends towards a limiting value of $\sum G_{00}/M$ and the dipole radiation varies as $\omega \sum G_{1m}/M$. Figure 11 shows the sound-pressure response reconstructed using monopole components only. The height of this baseline is set primarily by two or three of the low-order modes, such as the $T(1,1)_2$, which have both strong monopole radiativities and low effective masses. Note, however, that the baseline itself is governed by both the relative strengths and the *polarities* of the different G_{lm}, and it is clear that whilst coupling to some modes will raise the baseline, coupling to others will reduce it. It may well be that the particular baseline set by the low-order modes has a significant bearing on the balance between treble and bass response of the guitar. The maker has considerable control of the parameters governing these modes [37], and investigating their role in determining quality could be a fruitful area for further research.

The rising baselines seen in the reconstructions of Figure 9 are generated by the dipole contributions. Whilst similar comments can be made about $\sum G_{1m}/M$, the discussion is more complicated because of the directional nature of this radiation, but it is another area which possibly warrants further investigation. At higher frequencies, the modes increasingly have nodes which run along the bridge line (i.e. they have high effective masses at the bridge) and have mode shapes which are incompatible with strong

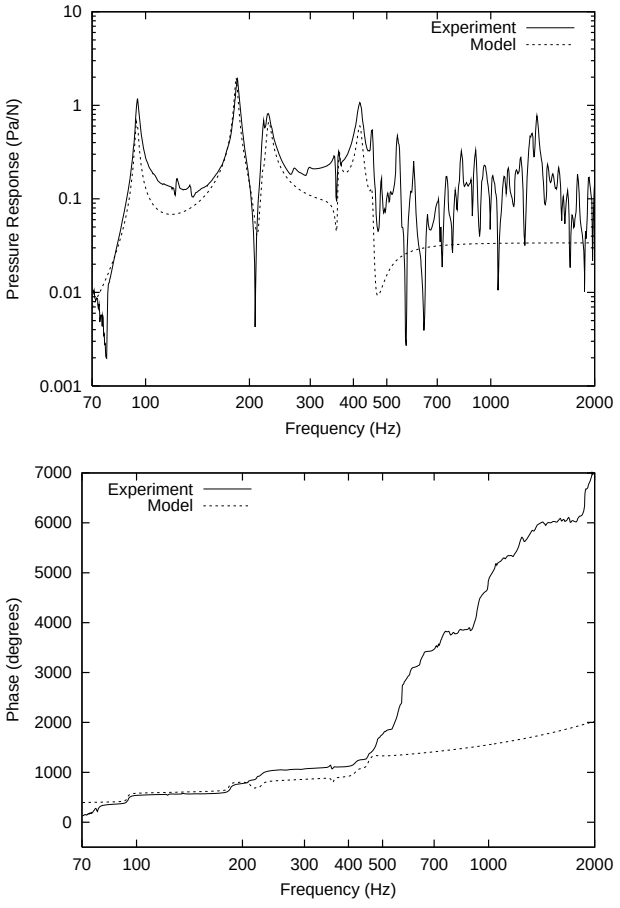

Figure 11. Measured and modelled sound-pressure response for $r = 0.45$ m, $\theta = 45°$, $\phi = -45°$ reconstructed using monopole sources only (cf. Figure 9c).

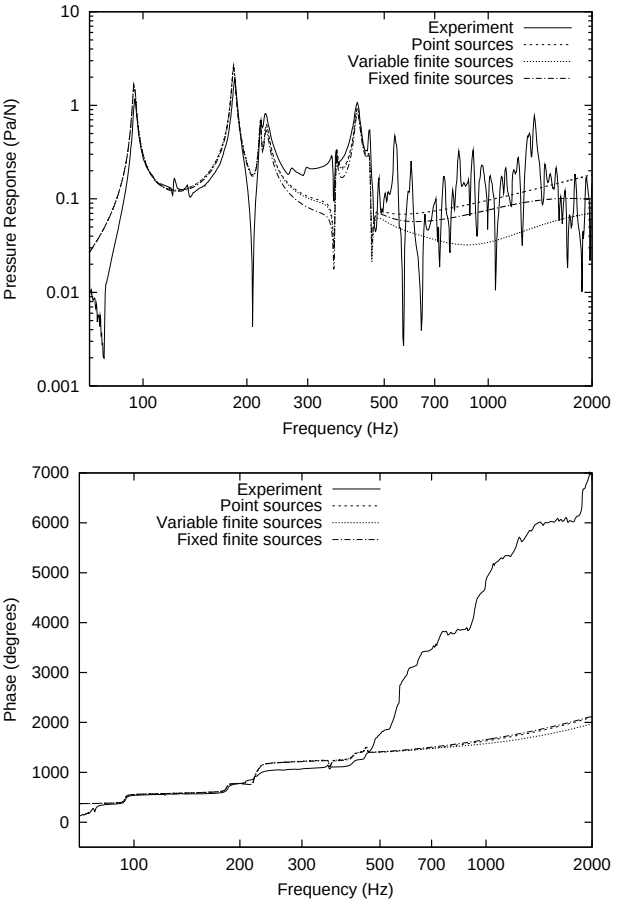

Figure 12. Measured and modelled sound-pressure response curves at $r = 0.45$ m, $\theta = 45°$, $\phi = -45°$. Data are reconstructed to compare point and finite sources.

monopole or dipole radiation. Consequently, these modes produce local variations in the radiated response, which, though adding interest and variety to the strengths of radiated string partials, are probably of less importance in determining absolute quality.

6.2. Finite-sized sources

The point-source model has certain advantages in the determination of the radiation components since it alleviates the requirement to specify source locations. (The penalty is that the determination of phase is then more difficult, particularly when working in the near field.) However, finite-sized sources can readily be included in the pressure reconstructions, which then give rather better fits to the mid-frequency baseline. In particular, they reverse the upward trend.

Equating standard theory for a pulsating sphere (monopole) and translating hard sphere (dipole) with equation (9) gives

$$G_{00} \equiv 4\pi {r_0}^2 \frac{\mathrm{e}^{-\mathrm{i}kr_0}}{1 - \mathrm{i}kr_0} \tag{14}$$

and

$$G_{1m} \equiv 4\pi {r_0}^3 \frac{\mathrm{e}^{-\mathrm{i}kr_0}}{2 - 2\mathrm{i}kr_0 - k^2{r_0}^2}, \tag{15}$$

where r_0 is the radius of the sphere. In the limit of $kr_0 \ll 1$ (the point-source limit) these reduce to $4\pi {r_0}^2$ and $2\pi {r_0}^3$ respectively, allowing the effective radii to be determined from the measured G_{00} and G_{1m}. There are no conceptual difficulties in dealing with the monopole components, because it is easy to see how the radial velocity of the pulsating sphere might notionally be equated with the normal velocity at the bridge. The calculated effective radii for the monopole sources are about 50 mm, rather smaller than might be anticipated from the general dimensions of the guitar. There is no similar equivalence with the dipole, where the translation of the hard sphere has no direct physical counterpart except, perhaps, for a dipole aligned along the x-axis. The alternative description of the dipole — a pair of closely-spaced pulsating spheres — is no more help in that a radius and separation must be determined independently. Calculated effective radii based on the translating hard sphere are again about 50 mm, giving sphere diameters which are consistent with the depths of the ribs in the guitar.

Figure 12 shows a comparison of experimental data with the point-source model, the variable-sized finite-source model and a fixed-size finite source-model. The latter is based on monopole-source radii of 150 mm and dipole-source radii of 50 mm. In general, the fixed-sized

finite sources give a good fit to the data, rolling over at about 1.6 kHz. The variable-sized finite sources generally give less good agreement, as shown here. The exact fit is very dependent on the individual source radii.

7. Conclusions

In this paper we have shown how the input admittance and sound-pressure response of the guitar can be characterised and reconstructed from a set of acoustical parameters, comprising resonance frequencies, Q-values, effective masses and orthogonal radiation components of a small set of low-order body modes. Comparatively little data are required to reproduce accurate detail in the frequency range up to about 600 Hz, and it has been shown that the average sound-pressure response above this range is determined largely by radiation from two or three "principal" modes excited above resonance. The response in these mid-frequency ranges is dependent on the magnitudes and polarities of the radiation coefficients as well as the effective masses of the modes. We have also demonstrated that dipole radiation is significant, even in the case of "air-pumping" modes previously thought to have basically omni-directional fields. Radiation components of higher order appear to play a less important role in the frequency range investigated. Data collected so far from a number of classical guitars are beginning to give some insight into the acceptable range of these acoustical parameters found amongst a set of "high-quality" instruments. These data would be suitable for constructing an extended model of the guitar, including strings, which could be used in psychoacoustical investigations.

Acknowledgement

The authors gratefully acknowledge financial support from the Leverhulme Trust (ref: F/407/R) and the EPSRC for a PhD studentship for SJR. We also acknowledge the assistance of Mr. D. Pickering for the construction of the hardware, Mr. C. R. Tucker for the design and assembly of the electronics and Dr. C. J. Evans for his assistance with the algorithm used for the spherical-harmonic decomposition.

References

[1] J. Meyer: Akustik der Gitarre in Einzeldarstellungen. Verlag E. Bockinsky, Frankfurt, 1985.

[2] O. Christensen: An oscillator model for analysis of guitar sound pressure response. Acustica **54** (1984) 289–295.

[3] M. Brooke: Numerical simulation of guitar radiation fields using the boundary element method. Dissertation. University of Wales, 1992.

[4] H. A. K. Wright: The acoustics and psychoacoustics of the guitar. Dissertation. University of Wales, 1996.

[5] H. A. K. Wright, B. E. Richardson: On the relationships between the response of the guitar body and the instrument's tone quality. Proc. Inst. Acoustics **19** (1997) 149–154.

[6] S. J. Richardson, T. J. W. Hill, B. E. Richardson: Theory and measurements of acoustical parameters for the characterisation of the function of the classical guitar. Proc. 7th International Congress on Sound and Vibration, Garmisch-Partenkirchen, Germany (2000) 1857–1864.

[7] T. J. W. Hill, B. E. Richardson, S. J. Richardson: Measurements of acoustical parameters for the classical guitar. Proc. International Symposium on Musical Acoustics, Perugia, Italy **2** (2001) 417–420.

[8] T. J. W. Hill, B. E. Richardson, S. J. Richardson: Input admittance and sound field measurements of ten classical guitars. Proc. Inst. Acoustics **24** (2002).

[9] S. J. Richardson: Acoustical parameters for the classical guitar. Dissertation. University of Wales, 2001.

[10] G. Caldersmith: Radiation from lower guitar modes. J. Guild of American Lutherie **2** (1985) 20–24.

[11] G. Caldersmith: Vibration geometry and radiation fields in acoustic guitars. Acoustics Australia **14** (1986) 47–51.

[12] B. E. Richardson: The acoustical development of the guitar. J. Catgut Acoust. Soc. **2**(5) (1994) 1–10.

[13] S. Berge, A. Chaigne, A. L. Pichon: Comparison between experimental and predicted radiation of a guitar. Acustica **84** (1998) 136–145.

[14] B. E. Richardson, M. Brooke: Modes of vibration and radiation fields of guitars. Proc. Inst. Acoustics **15**(3) (1993) 689–696.

[15] W. Y. Strong, T. B. Beyer, D. J. Bowen, E. G. Williams, J. D. Maynard: Studying a guitar's radiation properties with near-field holography. J. Guitar Acoust. **6** (1982) 50–59.

[16] L. M. Wang, C. B. Burroughs: Acoustic radiation from bowed violins. J. Acoust. Soc. Am. **110** (2001) 543–555.

[17] G. Weinreich, E. B. Arnold: Method for measuring acoustic radiation fields. J. Acoust. Soc. Am. **68** (1980) 404–411.

[18] E. B. Arnold, G. Weinreich: Acoustical spectroscopy of violins. J. Acoust. Soc. Am. **72** (1982) 1739–1746.

[19] G. Weinreich: Sound hole sum rule and the dipole moment of the violin. J. Acoust. Soc. Am. **77** (1984) 710–718.

[20] G. Weinreich: Radiativity revisited: theory and experiment ten years later. Proc. of Stockholm Music Acoustics Conference (SMAC 93), July 28 - August 1, 1993, Royal Swedish Academy of Music, Stockholm (1994) 432–437.

[21] G. Weinreich: Directional tone colour. J. Acoust. Soc. Am. **101** (1997) 2338–2346.

[22] P. M. Morse, K. U. Ingard: Theoretical acoustics. McGraw-Hill, NY, 1968.

[23] A. H. Stroud, D. Secrest: Gaussian quadrature formulae. 1st ed. Prentice Hall, London, 1966.

[24] E. G. Williams: Fourier acoustics. Academic Press, San Diego, CA, 1999.

[25] B. E. Richardson: A physical investigation into some factors affecting the musical performance of the guitar. Dissertation. University of Wales, 1982.

[26] C. J. Evans: Optimisation of passive shimming techniques for magnetic-resonance imaging. Dissertation. University of Exeter, 1999.

[27] R. Vadovic: Aspects concerning the choice of measurement points and specification of parameters needed for a proper determination of magnetic fields. IEEE Trans. Magnetics **28** (1992) 1826–1832.

[28] N. Giordano: Mechanical impedance of a piano soundboard. J. Acoust. Soc. Am. **103** (1998) 2128–2133.

[29] K. Marshall: Modal analysis of a violin. J. Acoust. Soc. Am. **77** (1985) 695–709.

[30] C. Lambourg, A. Chaigne: Measurments and modeling of the admittance matrix at the bridge in guitars. Proc. of Stockholm Music Acoustics Conference (SMAC 93), July 28 - August 1, 1993, Royal Swedish Academy of Music, Stockholm (1994) 448–453.

[31] X. Boutillon, G. Weinreich: Three-dimensional mechanical admittance: Theory and new measurement method applied to the violin bridge. J. Acoust. Soc. Am. **105** (1999) 3524–3533.
[32] D. J. Ewins: Modal testing: Theory and practice. 1st ed. Research Studies Press, Letchworth, UK, 1984.
[33] M. J. Elejabarrieta, A. Ezcurra, C. Santamaría: Coupled modes of the resonance box of the guitar. J. Acoust. Soc. Am. **111** (2002) 2283–2292.
[34] I. M. Firth: Physics of the guitar at the Helmholtz and first top plate resonances. J. Acoust. Soc. Am. **61** (1977) 588–593.
[35] O. Christensen: Quantitative models for low frequency guitar function. J. Guitar Acoust. **6** (1982) 10–25.
[36] O. Christensen: The response of played guitars at middle frequencies. Acustica **53** (1983) 45–48.
[37] B. E. Richardson: Simple models as a basis for guitar design. J. Catgut Acoust. Soc. **4**(5) (2002) 30–36.